Astron. Astrophys. 349, 295–300 (1999)

ASTRONOMY AND ASTROPHYSICS

Relationship between polarization and intensity of the green line in different coronal structures

O.G. Badalyan[1], **M.A. Livshits**[1], **and J. Sýkora**[2]

[1] Institute of Terrestrial Magnetism, Ionosphere and Radio Wave Propagation, 142092 Troitsk, Russia (badalyan/livshits@izmiran.troitsk.ru)
[2] Astronomical Institute, SK-05960 Tatranská Lomnica, Slovak Republic (sykora@ta3.sk)

Received 3 February 1999 / Accepted 17 June 1999

Abstract. The effect of anticorrelation between the polarization and intensity of the coronal green line Fe XIV 530.3 nm, revealed by the July 11, 1991 eclipse observations, is investigated. To simplify the general character of this effect, we have created the diagrams p versus $\log I_\lambda$ for the points inside a narrow ring, at fixed distances from the solar disk centre. In this case, the global anticorrelation dependence disintegrated into two branches with 'a void zone' between them. The subsequent analysis has shown that the points, corresponding to the individual coronal structures of different types, are clustered in specific places of the diagram. While the upper branch is related to the huge high-latitude streamers, the lower branch contains the equatorial coronal condensations of different brightness. These branches are best evident at the distance $\sim 1.2\ R_\odot$, and they vary with the distance from the disk centre. Model calculations, performed within the scope of generally accepted concepts, cannot explain the observed peculiarities of the anticorrelation dependence, in particular, the presence of the gap between the two branches. The way out of these difficulties could be sought in assuming that the coronal magnetic field affects the generation of the polarized radiation in the emission green line.

Key words: eclipses – Sun: corona – polarization – magnetic fields

1. Introduction

Measurement of the green line polarization offers considerable opportunity to study physical conditions in the solar corona, including the magnetic field. This paper represents a certain progress in our previous investigations, based on observations of the coronal green line polarization, performed during the July 11, 1991 solar eclipse (La Paz, Mexico), close to the phase of the solar cycle maximum (see Badalyan & Sýkora 1997a; Badalyan et al. 1997). The distribution of the polarization p and the line intensity I_λ for the whole corona was demonstrated and a new effect – the anticorrelation dependence between these two quantities, was revealed (Badalyan & Sýkora 1997a). Within this anticorrelation, the dependence of the degree of polarization on the density, temperature, and magnetic field topology of the source of the line radiation, are manifested in a rather complicated way.

The purpose of the present study is to investigate the observed anticorrelation effect in detail. For that reason, we have analysed the anticorrelation dependence for the points inside individual narrow rings, i.e., for the points at, approximately, the same distance ($\rho \approx const$). Applying this approach, the original anticorrelation dependence clearly splits into two branches. The affiliation of the different coronal structures to these branches, and the changes in the pattern of anticorrelation with the distance of the rings, are investigated. The physical meaning of the peculiarities found is discussed in Sect. 6.

2. Observational data

Our high-quality eclipse images of the green-line corona were taken with sufficiently high spatial resolution, by using a narrow band filter ($\Delta\lambda$ = 0.17 nm), and the polarizer turned step by step to four positions (Sýkora et al. 1994). In addition to that, three sets of the polarized white-light corona images were obtained with different exposures. All the images were photometrically processed, carefully preserving their spatial identification. The contribution of the white-light radiation, passing through the applied narrow-band filter, was subtracted from the total radiation detected in the green-line images. This procedure was carried out under the assumption that practically all the radiation detected on the green-line images in the region of the north-pole coronal hole is of the white-light corona origin.

The complete processing of observations provided a map of the distribution of polarization for the whole corona, the size of one pixel being $4.5''$. Analysis of this map revealed a number of peculiarities in the behaviour of the green-line polarization in different regions of the solar corona (Badalyan & Sýkora (1997a), Badalyan & Sýkora (1997b) and Badalyan et al. (1997). In order to get lower statistical scattering of the measurements, somewhat smaller averaged matrices were used in the present study (the size of the pixels was $15''$). Nevertheless, in our analysis we have sometimes used the higher resolution data, as well.

The shape of the white-light corona, visible on the eclipse day (Fig. 1), was distinctly different from the spherically symmetrical corona, typical for the solar maximum phase. Systems

Send offprint requests to: J. Sýkora

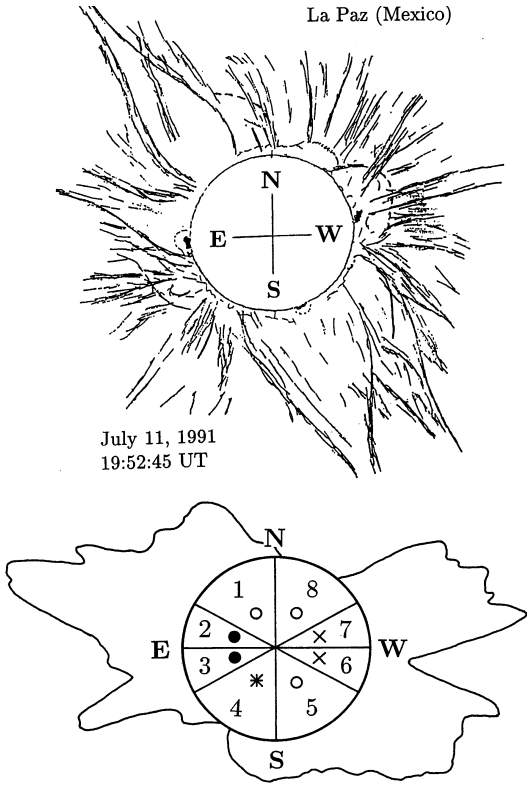

Fig. 1. The structure of the white-light corona, as observed during the July 11, 1991 solar eclipse (upper panel), and the brightness of the green-line corona (in relative units), as derived for the distance 1.2 $R_\odot$ (lower panel) from the data given in Badalyan & Sýkora (1997a). The same marks, as indicated inside the sector scheme here, are used in Figs. 2 and 4 of this paper. The position angles P of the sector boundaries are: 0° (north), 60°, 90° (east), 120°, 180° (south), 240°, 270° (west) and 300°.

of huge helmet streamers were detected in the high solar latitudes as a consequence of the specific orientation of the actual heliospheric current sheet. Coronal condensations present close to the equator, were not so well-developed, as usual for the periods of high solar activity. A distinct coronal hole was present in the vicinity of the north pole and, in addition to that, a region of decreased X-ray radiation, similar in its characteristics to the coronal hole, was observed at the position angles P around 150°. As usual, the direction of the position angles indication is N $\rightarrow$ E $\rightarrow$ S $\rightarrow$ W $\rightarrow$ N. Throughout this paper the P angles correspond to the north pole position shown in Fig. 1.

The distribution of the green-line corona brightness, derived from Fig. 3 of Badalyan & Sýkora (1997a), is shown in the lower part of Fig. 1. The out-eclipse green-line intensities, measured on the eclipse day $40''$ above the solar limb, were presented by Rušin et al. (1992). The images obtained by the Normal Incidence X-ray Telescope (NIXT) in the Fe XVI 63.7 Å line two and a half hour prior to the July 11, 1991 eclipse (Golub & Pasachoff 1997), were also used in our analysis of the limb activity.

3. Two branches of the anticorrelation dependence

The total green line intensity I_λ is the sum of two components, I_e and I_{ph}. The first originates due to excitation of the Fe XIV ion by electron collisions, and the second component appears because the ion is excited by the absorption of photospheric photons. The linear polarization in the λ 530.3 nm line is caused by scattering of the photospheric radiation only, i.e., it is related to the I_{ph} component. Since, in absence of the magnetic field, the angular distribution of the scattering in the line is analogous to that of the Thomson scattering, the intensities of the 'scattered' radiation in the line and in the white-light continuum are mutually proportional, if indeed, these two kinds of radiation originate in the same region of the corona. So, the polarization in the line can be expressed as follows (Badalyan & Livshits 1999, private communication):

$$p = a(T)\frac{\sigma_{5303}}{\sigma}\frac{p_{ph}B_{wl}}{I_\lambda}, \qquad (1)$$

where $a(T)$ is the relative abundance of the Fe XIV ion, and σ and σ_{5303} are coefficients of the scattering in the white-light and green line radiations, respectively. In Eq. (1) the quantity p_{ph} represents the degree of polarization of the scattered radiation in the resonance lines, in our case, the forbidden line. This quantity can be calculated theoretically. The product $p_{ph}B_{wl}$ practically represents the polarized brightness of the white-light corona.

Eq. (1) describes the anticorrelation relation which statistically appeared when the measurements over the whole corona were analysed together (Badalyan & Sýkora 1997a). This inverse proportionality should be more clearly expressed if only the points with constant $p_{ph}B_{wl}$ are considered (in the inner corona, this condition is fulfilled for the points at the same distance from the disk centre).

The relatively wide p versus $\log I_\lambda$ band of points, representing the anticorrelation in Fig. 4a of Badalyan & Sýkora (1997a), includes the dependence of the degree of polarization on the distance, as well as, on the morphological variety of coronal structures around the limb.

To understand the role of coronal structures, we have prepared the p versus $\log I_\lambda$ diagram for the set of points inside a narrow ring 0.05 $R_\odot$ wide, at a distance $\rho = 1.2\,R_\odot$. The relevant diagram is shown in Fig. 2. We restricted ourselves to the most reliably measured values with $\log I_\lambda > 0.6$. Fig. 2 clearly shows that the original wide band of points, characteristic for the corona as a whole, separates into two distinct branches with a noticeable gap between them.

To disclose regularities in the distribution of the points on the p–$\log I_\lambda$ diagram, we divided the whole solar corona into 8 sectors, according to the heliographic latitudes, or the position angles (see Fig. 1). The sector boundaries approximately separate the zones of the huge high-latitude streamers from the equatorial zone. Activity in the equatorial zone is weakly pronounced, though several coronal condensations are recognized on the Fe XVI 63.7 Å line images (Golub & Pasachoff 1997). The same properties of the green corona brightness were recorded at a height $40''$ above the limb (see Fig. 2 in Rušin et al. 1992).

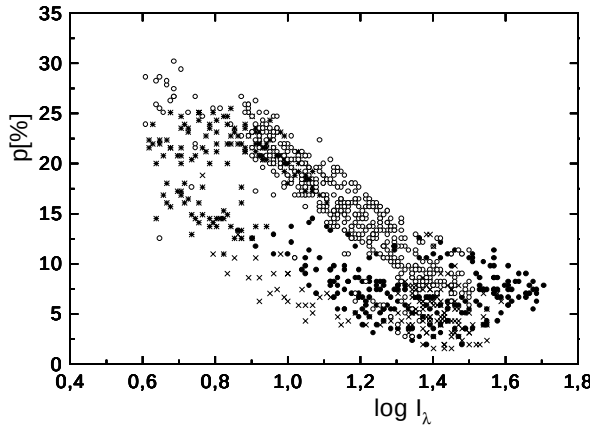

Fig. 2. The anticorrelation dependence for the set of points inside the ring 0.05 $R_\odot$ wide, at the distance 1.2 $R_\odot$. White circles are related to the Sectors 1, 5 and 8 (they include regions of the high-latitude streamers and several points around the north-pole coronal hole); black circles – Sectors 2 and 3 (eastern equatorial regions); crosses – Sectors 6 and 7 (western equatorial regions); asterisks – Sector 4 (a part of the eastern equatorial region, the southern coronal hole, and a part of the southern streamer, successively).

The measurements related to the different sectors are indicated in Fig. 2, as follows: The white circles indicate the NE– and SW–sectors (No. 1 and No. 5), where the high-latitude streamers occur, together with a small number of points from the NW–sector (No. 8), representing the north-pole coronal hole and the neighbouring regions. The two eastern equatorial sectors (Nos. 2 and 3) are marked by the black circles, and two western equatorial sectors (Nos. 6 and 7) are indicated by the crosses. Finally, the SE–sector (No. 4, asterisks) includes the southern boundary of the equatorial region, the southern region of the decreased brightness (probably, a coronal hole), and the eastern part of the southern streamer. The points related to sector No. 4, show a gradual transition from the lower branch to the upper one, at the low values of $\log I_\lambda$.

Inspection of the data from the sectors leads us to the general conclusion that the upper branch is mainly related to the huge high-latitude streamers, while the lower branch is related to the equatorial regions. We have also noticed that the large-scale structures of the same type are distributed in different parts of the corresponding branch. For example, as can be deduced from Fig. 1, the northern and southern streamers are different, the southern streamer being broader, representing a system of several streamers in the layers close to the plane of the sky. Due to this, the points referring to the southern streamer occupy a relatively large range of intensities, while, the northern streamer is limited within $1.1 < \log I_\lambda < 1.3$.

The range of the degree of polarization variations reaches 5–7%, in each of the branches. Such a dispersion follows from a number of factors, such as the physically real differences of the p values (arising from overlapping of the different coronal structures; the finite, though small, width of the chosen ring; actual variations of the degree of polarization within a given structure), as well as the statistical dispersion of the measured data.

4. Anticorrelation dependence in different large-scale coronal structures

For a more detailed study of the clouds of points, pertaining in the p–$\log I_\lambda$ diagram to the different large-scale coronal structures, we chose an even narrower ring – 0.03 $R_\odot$ wide. Fig. 3a shows a gradual shift along the upper branch and crossing to the lower branch for the sectors No. 5 and No. 6 (black circles), i.e. across the SW−streamer to the south-west equatorial region (black circles). The points are linked by lines, in accordance with the position angle increase. The region with the lowest polarizations and the highest intensities in Fig. 3a corresponds to that region in Fig. 1 where the upper boundary of the southern system of streamers (around $P = 240°$), above the bright emission in Fe XVI, traverse to the fine coronal structures close to the west equator, above the weak Fe XVI emission (Golub & Pasachoff 1997). Almost all the data obtained from the system of southern streamers is displayed in Fig. 3a. The principal upper cloud of points (near $P \leq 207°$) belongs to the huge near-pole streamer, close to the plane of the sky. Somewhat lower, another cloud of points belongs to the region where two streamers overlap in Fig. 1, and then, the transition to the second streamer takes place at $P \geq 217°$.

The isolated NE–streamer is represented by the points with $P = 20° - 56°$. For the distance of 1.2 $R_\odot$, the corresponding points are displayed in the upper branch of Fig. 2 within $1.1 < logI_\lambda < 1.3$ and $12\% < p < 20\%$. (The parameters of the NE–streamer are presented in Fig. 5, for four different distances). In Fig. 3c this northern streamer is shown at the distance 1.175 $R_\odot$, together with some other structures. It should be noticed that the intervals $\Delta \log I_\lambda$ for the northern and the near-pole southern streamer (i.e., for its part outside the overlapping of the two streamers), are approximately equal.

Fig. 3b illustrates the measurements from the east limb: two brightness maxima (see the lower part of Fig. 1), related to the coronal condensations at $67° < P < 80°$ (black triangles) and $107° < P < 115°$ (white triangles), and the equatorial regions of medium activity at $84° < P < 108°$ (black circles) and $119° < P < 129°$ (white circles). Comparison with Fig. 2 reveals that these four groups of points are all on the lower branch of the diagram, representing fairly low polarizations. Two coronal condensations at $225° < P < 257°$ and $273° < P < 300°$, and the western equatorial region at $259° < P < 269°$, are also displayed in the lower branch. All the points in the enumerated intervals of position angles create different clusters in the diagram. Thus, as earlier in the case of the coronal streamers, the coronal condensations and the equatorial features of increased activity are also displayed in the same, now the lower, branch of the anticorrelation diagram.

Obviously, our method of the white-light contribution subtraction from the green line polarization eliminated any information about the central parts of coronal holes. Nevertheless, we found it possible to study, at least, the regions in the neighbour-

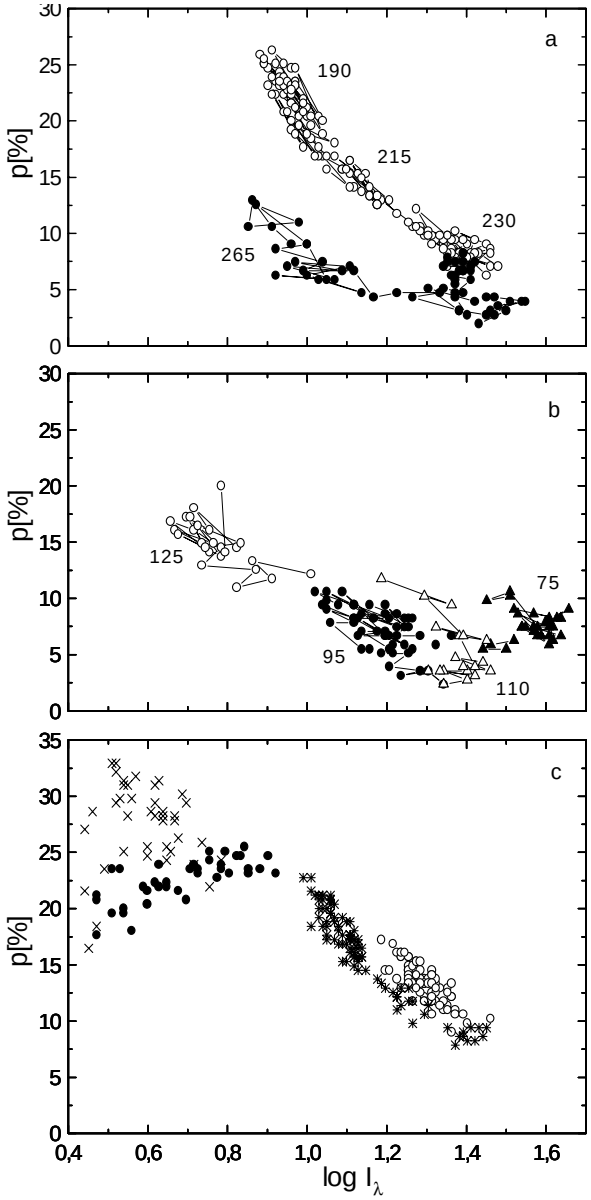

Fig. 3a–c. The anticorrelation dependence for the different large-scale coronal structures (numbers indicate the position angles): **a** The system of the southern streamers (Sector 5, white circles) and the regions of the south-west limb (Sector 6, black circles), both at the distance 1.2 $R_\odot$; **b** The coronal condensations of different brightness, present on the east limb at the distance 1.2 $R_\odot$; **c** Northern (white circles) and southern (asterisks) streamers, together with the northern (crosses) and south-eastern (black circles) coronal holes, both pairs at the distance 1.175 $R_\odot$.

hoods of the holes (in the case of the south-east region, in the neighbourhood of a feature similar to a hole) by analysing the points with low green line intensities. So, to study the coronal holes, the points with $0.60 > \log I_\lambda > 0.44$ were also considered. However, accuracy in this case decreases, and the results obtained should be viewed cautiously.

The p–$\log I_\lambda$ dependence of the two quasi coronal holes, is presented in Fig. 3c. Two high-latitude streamers are added to this figure to demonstrate the position of the holes in the diagram relative to the original branches shown in Fig. 2. Fig. 3c was constructed from points inside the ring at a distance 1.175 $R_\odot$. Here, the white circles indicate the northern streamer ($20° < P < 56°$), the asterisks relate to the southern streamer ($164° < P < 225°$), the black circles indicate the south-east coronal hole ($133° < P < 164°$) and the crosses belong to the northern hole ($P < 10°, P > 320°$). According to Fig. 3c, the coronal holes are distributed in the region of the low intensities and large polarizations in the original diagram (Fig. 2), joining both the branches in the range of low $\log I_\lambda$ values. The southern hole is somewhat brighter, with the degrees of polarization somewhat lower, in comparison with the northern hole and, apparently, this hole occupies a larger range of intensities. Notice the clearly separated positions of the two streamers in Fig. 3c.

The above analysis of the Figs. $2-3$ gives reasons to suppose that each of the branches consists of the individual clouds of points, related to the single structures of the same type. The clustering of the points within the branches into the separated clouds becomes even more evident if the p–$\log I_\lambda$ diagrams are constructed from the unsmoothed intensity and polarization matrices (600×600 in size, with one pixel being $4.5"$). With these large matrices, extremely narrow rings (down to 0.005 $R_\odot$ wide) can be analysed, and any dependence of the polarization and intensity on the distance is completely eliminated. Consequently, a much stronger concentration of the points throughout the diagrams, particularly for the northern streamer and the basic (not overlapping) part of the southern streamer at $164° < P < 207°$, is observed.

5. Variations of the anticorrelation diagram with distance

The July 11, 1991 eclipse was prolonged, more than six minutes in duration. Therefore, the lowest coronal layers were obscured by the Moon. Images of the green-line corona were taken during the first half of the eclipse. That is why the west solar limb was obscured more than the east one. Overall, the regions at a distance $\rho > 1.08\, R_\odot$ on the east limb and $\rho > 1.15\, R_\odot$ on the west limb, were accessible for the measurements. Therefore, anticorrelation diagrams can be constructed for the complete rings at a range of distances 1.15 – 1.30 $R_\odot$. With the small distances, there are less points at the west limb, and the lower branch is worse defined. Both the branches are best visible within the distances 1.17 – 1.27 $R_\odot$

Figs. 4a and 4b show the anticorrelation dependence for the distances 1.175 $R_\odot$ and 1.27 $R_\odot$, respectively. In both cases, the rings were 0.03 $R_\odot$ wide and the low intensity regions are also included. The mutual comparison of Fig. 4a with Fig. 4b reveals that the right-hand side of the diagram, where both the branches join, shifts to the lower intensities with enlarging ρ. At larger distances (Fig. 4b), the upper branch becomes more inclined than the lower branch. While in Fig. 4a both the branches are almost parallel, in Fig. 4b their inclinations are remarkably different. At the distance 1.30 $R_\odot$ (the corresponding figure is not shown here) a certain number of points also occur in the region between the branches. Nevertheless, as earlier, we are still

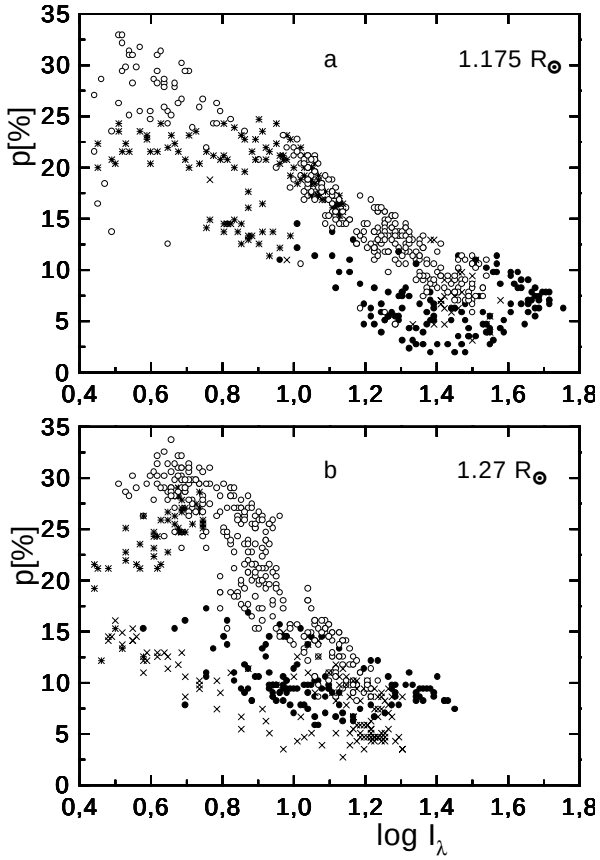

Fig. 4a and b. The anticorrelation diagrams for two rings at the indicated distances. The marks used are the same as in Fig. 2.

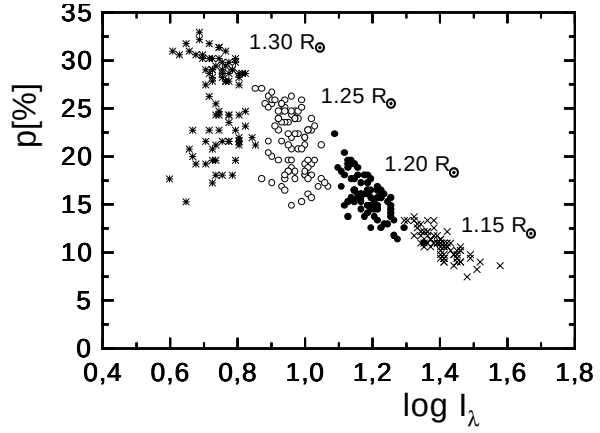

Fig. 5. Polarizations and intensities of the NE−streamer, as measured at different distances: 1.15 $R_\odot$ (crosses), 1.20 $R_\odot$ (black circles), 1.25 $R_\odot$ (white circles), and 1.30 $R_\odot$ (asterisks).

capable of identifying the regions related to the high-latitude streamers and to the near-equatorial regions. At the distance 1.30 $R_\odot$, the branch related to the equatorial regions becomes practically horizontal.

Variations of the anticorrelation dependence with the distance ρ can also be analysed for the individual coronal structures. For example, we present this dependence for the well-isolated NE–streamer, at four discrete distances: 1.15, 1.20, 1.25, and 1.30 $R_\odot$ (see Fig. 5). For each of the distances, the points are clearly clustered. Generally, Fig. 5 manifests the well-known variation of the polarization with the distance from the disk centre (see Picat et al. 1979; Badalyan & Sýkora 1997b; Badalyan et al. 1997). Fig. 5 indicates that the dispersion of the points along the p axis increases with distance. Nevertheless, a more detailed study reveals that the vertical sizes (the range of p) of the four clouds of points are more connected with the real changes of the polarization p along the limb, than with the statistical dispersion of the measurements. The mean square deviation of the p values from the averaged curve is approximately equal at all the distances and is $\sim 1.5\%$.

The comparison of Figs. 2 and 4 shows that, even over a rather small interval of the distances, the anticorrelation diagrams change remarkably. All the coronal structures show, however, similar variations with the distance, as presented in Fig. 5 for the NE–streamer. Therefore, any common presentation of all the data from all the distances within one diagram, obscures the real anticorrelation and leads to blurring of the two branches (this was the case in Fig. 4 in Badalyan & Sýkora (1997a).

6. Concluding remarks

The decrease of the degree of polarization, caused by the increasing role of electron collisions in the excitation of the coronal emission line, is the reason for the appearance of the anticorrelation dependence (see Eq. (1)). We have found that, for the points inside the narrow ring, the general anticorrelation breaks down into two branches with 'a void zone' between them. These two branches correspond to the streamers and the equatorial zones, respectively. Each of the branches represents a set of different clouds of points, related to the isolated large-scale coronal structures of the same type within the given branch.

Fig. 7 of Picat et al. (1979), in which practically all the preceding measurements were collected, indicates the higher degree of polarization in the streamers than in the active equatorial regions, and a certain difference in the rates of polarization p with the distance can be noticed within the two mentioned groups of the large-scale structures. Our discovery of the two separate branches in the p–$\log I_\lambda$ anticorrelation dependence represents significant progress in understanding the coronal green line polarization.

The position of any point in the p–$\log I_\lambda$ diagram depends, of course, on the model of a given coronal structure, primarily, on the adopted density, determining the contribution of the unpolarized component I_e. The global, rather obscured character of the anticorrelation dependence and, mainly, the presence of the two branches in it, do not allow explanation of the observed peculiarities within the scope of the generally accepted models of coronal structures (Badalyan 1999; Badalyan & Livshits 1999, private communication). It is difficult to explain the presence of 'the void zone' in the diagram, in other words, the jump-like transition from one branch to the another, at the same intensity.

Promisingly, one of the possible factors affecting the degrees of polarization and intensities of the coronal green line, is the

magnetic field. It seems reasonable to assume that the coronal structures, present in the same branch, have similar magnetic configurations, which leads to the nearly equal p_{ph} values. In fact, Eq. (1) indicates a strong dependence of the global polarization p from its p_{ph} component. To this effect, the presence of the two branches could be due to generation of the polarized green line radiation in the structures characteristic of substantially different magnetic field configurations. The calculations, considering the idealized magnetic field topology (i.e., the radial or dipole fields), were performed earlier (House 1974; House et al. 1982). Our results indicate the necessity of the modified calculations of polarization in the coronal emission lines, considering more realistic magnetic field configurations, taking into account more accurate density distributions in the corona.

Acknowledgements. This work was supported by the Grant No. 96-02-18383 of the Russian Foundation for Basic Research and by the VEGA Grants 02/5007/98 and 02/5017/98 of the Slovak Academy of Sciences.

References

Badalyan O.G., 1999, AZh 76, 225 (Astronomy Reports 43, 191)
Badalyan O.G., Sýkora J., 1997a, A&A 319, 664
Badalyan O.G., Sýkora J., 1997b, In: Mouradian Z., Stavinschi M. (eds.) Theoretical and Observational Problems Related to Solar Eclipses. Kluwer, Dordrecht, p. 25
Badalyan O.G., Livshits M.A., Sýkora J., 1997, AZh 74, 767 (Astronomy Reports 41, 682)
Golub L., Pasachoff J.M., 1997, The Solar Corona. Cambridge Univ. Press, Cambridge, cover illustration
House L.L., 1974, PASP 86, 490
House L.L., Querfeld Ch.W., Rees D.E., 1982, ApJ 255, 753
Picat J.P., Felenbok P., Fort B., 1979, A&A 75, 176
Rušin V., Klocok Ľ., Zimmermann P., et al., 1992, Contrib. Astron. Obs. Skalnaté Pleso 22, 117
Sýkora J., Rybák J., Ambrož, P., 1994, In: Rušin V., Heinzel P., Vial J.-C. (eds.) IAU Colloq. 144, Solar Coronal Structures. Veda, Bratislava, p. 541